

修士論文  
BELLE実験における  
タウ粒子の寿命の測定  
(A measurement of tau lifetime  
at BELLE experiment)

東北大学大学院理学研究科  
物理学専攻

野崎 聡

平成 16 年

### **Abstract**

We present a measurements of the tau lepton lifetime using data collected with the Belle detector at the KEKB asymmetric,  $3.5\text{GeV} \times 8.0\text{ GeV}$ ,  $e^+e^-$  collider. The lifetime is measured to be

$$\tau = (295.62 \pm 0.64 \pm 2.10) \times 10^{-15} s$$

using  $98.9\text{ fb}^{-1}$  data set.

# Contents

<b>1</b>	<b>Introduction</b>	<b>7</b>
1.1	The Tau Lepton . . . . .	7
1.2	The Tau Lepton decay and Lifetime . . . . .	8
1.3	Current status of Tau Lepton Lifetime . . . . .	9
<b>2</b>	<b>KEK B-factory</b>	<b>11</b>
2.1	KEKB accelerator . . . . .	11
2.2	Belle detector . . . . .	12
2.2.1	Silicon Vertex Detector(SVD) . . . . .	14
2.2.2	Central Drift Chamber (CDC) . . . . .	15
2.2.3	Aerogel Čerenkov Counter (ACC) . . . . .	17
2.2.4	Trigger/Time of Flight counter (TSC/TOF) . . . . .	18
2.2.5	Electromagnetic Calorimeter(ECL) . . . . .	20
2.2.6	$K_L/\mu$ detector (KLM) . . . . .	22
2.2.7	Extreme Forward Calorimeter (EFC) . . . . .	22
2.2.8	Trigger and Data Acquisition system (DAQ) . . . . .	22
2.3	Software . . . . .	26
2.3.1	Overview . . . . .	26
2.3.2	Monte Carlo simulator . . . . .	28
<b>3</b>	<b>Analysis</b>	<b>29</b>
3.1	Lifetime measurement method . . . . .	29
3.1.1	Proper Decay Length . . . . .	29
3.1.2	Decay Length Reconstruction . . . . .	31
3.1.3	Measuring the mean lifetime . . . . .	31
3.1.4	Calculating the lifetime . . . . .	33
3.2	The data set . . . . .	35
3.3	Event selection . . . . .	35
3.3.1	$\tau$ pair event selection . . . . .	35
3.3.2	Event Topology . . . . .	36
3.3.3	Event quality . . . . .	36

<i>CONTENTS</i>	3
3.3.4 Background rejection . . . . .	37
3.4 A Comparison of data with Monte Carlo . . . . .	41
3.5 Estimate the Background event fraction . . . . .	44
3.6 Correction . . . . .	44
3.7 Lifetime calculation . . . . .	46
3.8 Systematic Errors . . . . .	47
3.8.1 Interaction Point (IP) and Vertex . . . . .	48
3.8.2 Background fraction and lifetime . . . . .	48
3.8.3 Summary . . . . .	48
<b>4 Conclusion</b>	<b>49</b>
<b>Bibliography</b>	<b>51</b>
<b>Acknowledgments</b>	<b>53</b>

# List of Figures

1.1	Production of $\tau$ leptons by one-photon exchange. . . . .	7
1.2	Feynman diagram for $\tau$ decay mode . . . . .	8
1.3	Lifetime in other facilities . . . . .	10
2.1	Configuration of the KEKB strage ring. . . . .	13
2.2	Sideview of Belle detector. . . . .	14
2.3	Definition of Belle coordinate system. . . . .	15
2.4	Silicon vertex detector. . . . .	16
2.5	Central drift chamber. . . . .	17
2.6	Barrel aerogel Čerenkov counter. . . . .	18
2.7	Endcap aerogel Čerenkov counter. . . . .	19
2.8	Time of flight and trigger scintillator counters. . . . .	20
2.9	Electromagnetic calorimeter . . . . .	21
2.10	Schematic view of barrel KLM. . . . .	23
2.11	Schematic view of endcap KLM. . . . .	24
2.12	Extreme forward calorimeter. . . . .	25
2.13	Logic diagram of Belle trigger system . . . . .	27
2.14	Logic diagram of Belle Data Acquisiyion system . . . . .	27
3.1	Decay Length of MC . . . . .	30
3.2	Schematic view of tau decay vertex . . . . .	31
3.3	Proper decay length of MC . . . . .	32
3.4	. . . . .	37
3.5	Scatter plots of $P_T^*$ -vs- $P_Z^*$ plane. . . . .	38
3.6	Angle of Missing momentum direction . . . . .	38
3.7	The invariant mass distribution of three prong side . . . . .	39
3.8	Average opening angle distribution . . . . .	40
3.9	reconstructed theta distribution. Data are indicated by points with error bars, Monte Carlo by the solid histogram . . . . .	42
3.10	reconstructed tau distribution.Data are indicated by points with error bars, Monte Carlo by the solid histogram . . . . .	42

3.11	reconstructed two-dimensional decay length distribution. Data are indicated by points with error bars, Monte Carlo by the solid histogram	43
3.12	Proper decay length of background events . . . . .	45
3.13	Decay length distribution . . . . .	47
4.1	Comparison the result with other facilities results . . . . .	50

# List of Tables

2.1	Parameters of KEKB (number in the brackets are design value.) . . .	12
3.1	Summary of event Selection . . . . .	35
3.2	Event fraction of background . . . . .	44
3.3	List of input parameter . . . . .	46
3.4	List of systematic errors . . . . .	48

# Chapter 1

## Introduction

### 1.1 The Tau Lepton

The tau lepton is a member of third generation of lepton family. We know that tau mass is  $1.777\text{GeV}/c^2$ , its spin is  $\frac{1}{2}$  and that its decays, as those of muon, are mediated by the  $V - A$  interaction. Furthermore, the tau is known as the only lepton which is heavy enough to decay hadronically.

The only abundant sources of tau lepton to date have been  $e^+e^-$  colliders. Tau leptons are produced in  $e^+e^-$  collision via one-photon exchange (figure 1.1) and first observed in 1975 at the Stanford Positron-Electron Asymmetric Ring (SPEAR).

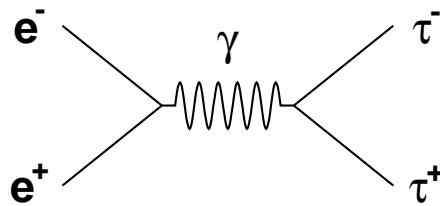


Figure 1.1: Production of  $\tau$  leptons by one-photon exchange.

## 1.2 The Tau Lepton decay and Lifetime

The possible decay modes for the tau are shown in Figure 1.2. The tau is heavy enough to decay hadronically. There is no general method for calculating the decay width and the semileptonic decay modes. But leptonic decays ( $\tau^- \rightarrow l^- \bar{\nu}_l \nu_\tau$ ) are

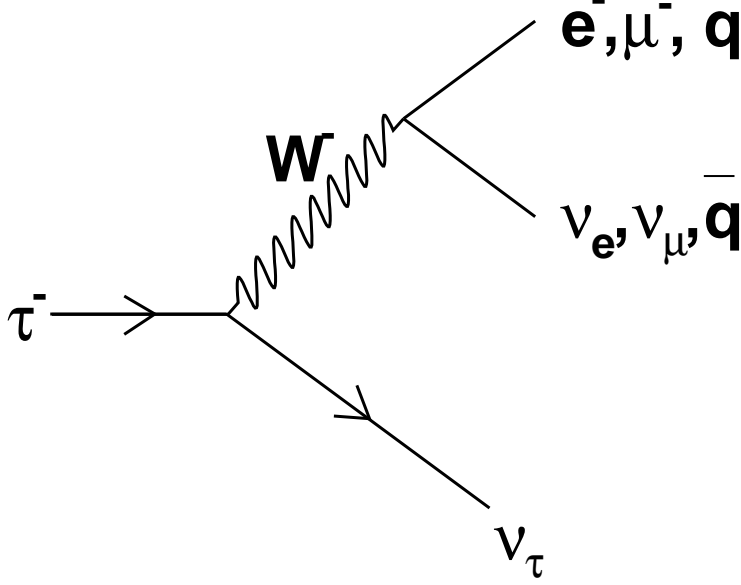


Figure 1.2: Feynman diagram for  $\tau$  decay mode

understood at the level of the electroweak radiative correction. Within the standard model,

$$\Gamma(\tau^- \rightarrow l^- \nu_\tau \bar{\nu}_l) = \frac{G_F^2 m_\tau^5}{192\pi^3} f\left(\frac{m_l^2}{m_\tau^2}\right) r_{EW} \quad (1.1)$$

where  $f(x) = 1 - 8x + 8x^3 - x^4 - 12x^2 \log x$ ,  $G_F = (1.16637 \pm 0.00001) \times 10^{-5} \text{ GeV}^{-2}$  is Fermi coupling constant,  $m_\tau$  is the  $\tau$  mass, and  $m_l$  is the mass of lepton ( $e$  or  $\mu$ ).  $\nu_\tau$  mass has been neglected.

The factor  $r_{EW}$  is a correction factor not included in the Fermi coupling constant  $G_F$ . And  $r_{EW}$  is defined as (Ref [3]),

$$r_{EW} = \left[ 1 + \frac{3}{5} \frac{m_\tau^2}{m_W^2} \right] \left[ 1 + \frac{\alpha(m_\tau)}{2\pi} \left( \frac{25}{4} - \pi^2 \right) \right] \quad (1.2)$$

with  $\alpha^{-1}(m_\tau) \simeq 133.3$ ,  $m_W = (80.425 \pm 0.038) \text{ GeV}/c^2$  is mass of  $W^\pm$  boson. We obtain

$$r_{EW} = 0.996 \quad (1.3)$$

using equation 1.2.

The tau lifetime is simply related to this width through the electron branching fraction

$$\tau_\tau = \frac{1}{\Gamma_{tot}} = \frac{B(\tau \rightarrow l\nu_l\nu_\tau)}{\Gamma(\tau \rightarrow l\nu_l\nu_\tau)}. \quad (1.4)$$

Using the World average branching fraction  $B(\tau \rightarrow e\nu_e\nu_\tau) = (17.84 \pm 0.06)\%$ , and mass  $m_\tau = (1776.99^{+0.29}_{-0.26})\text{MeV}/c^2$ , we obtain the Standard Model predicted lifetime,

$$\tau_\tau = (291 \pm 1) \times 10^{-15} \text{sec}. \quad (1.5)$$

### 1.3 Current status of Tau Lepton Lifetime

The  $\tau$  lifetime is measured in several facilities. A comparison the Standard Model predicted tau lifetime with recent experiment results are shown in figure 1.3 .

The current world average for the tau lifetime,

$$(290.6 \pm 1.1) \times 10^{-15} \text{sec} \quad (1.6)$$

is  $0.27 \sigma$  away from the SM predicted value.

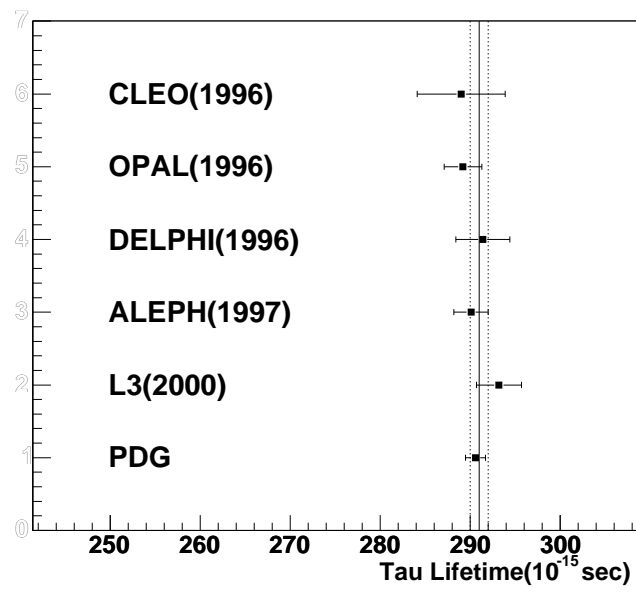


Figure 1.3: List of measured tau lifetime result. Standard Model predicted lifetime is also shown(line).

## Chapter 2

# KEK B-factory

The measurements of  $CP$  violation is main subject of BELLE experiment. The accelerator and detector are optimized to satisfy the physics requirement of the  $CP$  violation researches. But they are useful for the research of  $\tau$  physics. In this chapter, we give the description of the KEKB accelerator, Belle detector and the software system we used in this study.

### 2.1 KEKB accelerator

KEKB accelerator, located in Tsukuba, Japan is an asymmetric high luminosity  $e^+e^-$  collider. The accelerator is designed to have two separate rings for  $e^+$  and  $e^-$  beams because each of them has different beam energy. They are located in the TRISTAN tunnel as shown in Figure 2.1.  $e^+$  and  $e^-$  beams are accelerated by linear accelerator and injected into main ring at Fuji area. The  $e^+$  beam circulates inside of low energy ring (LER) anti-clockwise with the energy of 3.5 GeV, and the  $e^-$  beam circulates inside of high energy ring (HER) clockwise with the energy of 8.0 GeV. Both of the orbit length are about 3 km. The RF cavities which make up energy to the beams are installed at Nikko and Oho area for HER and at Fuji area for LER. The beams have two crossing points at Tsukuba and Fuji experimental hall, and are made to collide at the interaction point in the Tsukuba experimental hall, where the Belle detector is furnished.

The center of mass energy  $\sqrt{s}$  is 10.58 GeV. This is equal to the invariant mass of  $\Upsilon(4S)$  which decays into  $B\bar{B}$  pairs mainly. At this energy region,  $\tau$  pairs are created from  $e^+e^-$  in QED processes with the cross section of 0.91 nb. This is almost the same number of  $\Upsilon(4S)$  creation, we can get as many  $\tau$  samples as  $B\bar{B}$ .

The designed value and achieved record of KEKB parameters are listed in Table 2.1. A unique feature is that  $e^+e^-$  collide at a small angle  $\theta_x$ , in order to reduce parasitic collisions near the IP. As of December 2001, the achieved luminosity is  $5.4 \times 10^{-33}$ ,

Parameters	LER	HER	Units
Particles	$e^+$	$e^-$	
Energy ( $E$ )	3.5	8.0	GeV
circumstance ( $C$ )	3016.26		m
Luminosity ( $L$ )	$5.466 \times 10^{-33}$ ( $1 \times 10^{-34}$ )		$\text{cm}^{-2}\text{s}^{-1}$
Crossing angle ( $\theta_x$ )	$\pm 11$		mrad
Tune shifts ( $\xi_x/\xi_y$ )	0.039/0.052		
Beta function at IP ( $\beta_x^*/\beta_y^*$ )	0.33/0.01		
Beam current ( $I$ )	1.2 (2.6)	0.8 (1.1)	A
Natural bunch length ( $\sigma_z$ )	0.4		cm
Energy spread ( $\sigma_E/E$ )	$7.1 \times 10^{-4}$	$6.7 \times 10^{-4}$	
Bunch spacing ( $s_B$ )	0.59		m
Particles/bunch	$3.3 \times 10^{10}$	$1.4 \times 10^{10}$	
Emittance ( $\epsilon_x/\epsilon_y$ )	$1.8 \times 10^{-8}$ / $3.6 \times 10^{-10}$		m

Table 2.1: Parameters of KEKB (number in the brackets are design value.)

the half of the design value but highest in the world. The achieved beam currents are 1.2 A for the LER and 0.8 A for HER. The achieved LER current is much lower than design value. This is because the positron bunch is fattened by the background electron in the pipe. To avoid this, we set the coils around the LER beam pipe to attract the electron to the wall of the pipe. According to this operation, we are able to set high LER current without getting the positron bunch size larger.

## 2.2 Belle detector

The figure 2.2 show the overview of Belle detector. The Belle detector makes precise measurements of charged and neutral particles. The detector components dedicated for this analysis are a silicon vertex detector (SVD)[5], a central drift chamber (CDC)[6], an array of 1188 aerogel Čerenkov counter (ACC)[7], 128 time-of-flight scintillation counters (TOF)[8], and an electromagnetic calorimeter containing 8736 CsI(Tl) crystals (ECL)[9], all located inside the superconducting solenoid that generates a 1.5 T magnetic field. An iron return yoke outside the solenoid is segmented into 14 layers of 4.7-cm-thick iron plates alternating with a system of resistive plate counters that is used for identification of muons and detection of  $K_L^0$  mesons (KLM)[10], and an extreme forward calorimeter (EFC) containing 160 BGO( $\text{Bi}_4\text{Ge}_3\text{O}_{12}$ ) crystals n each end is placed around the beam line. Brief descriptions of the sub-detectors are given in the following subsections. Note that the coordinate system used in this dissertation is defined as Figure 2.3.

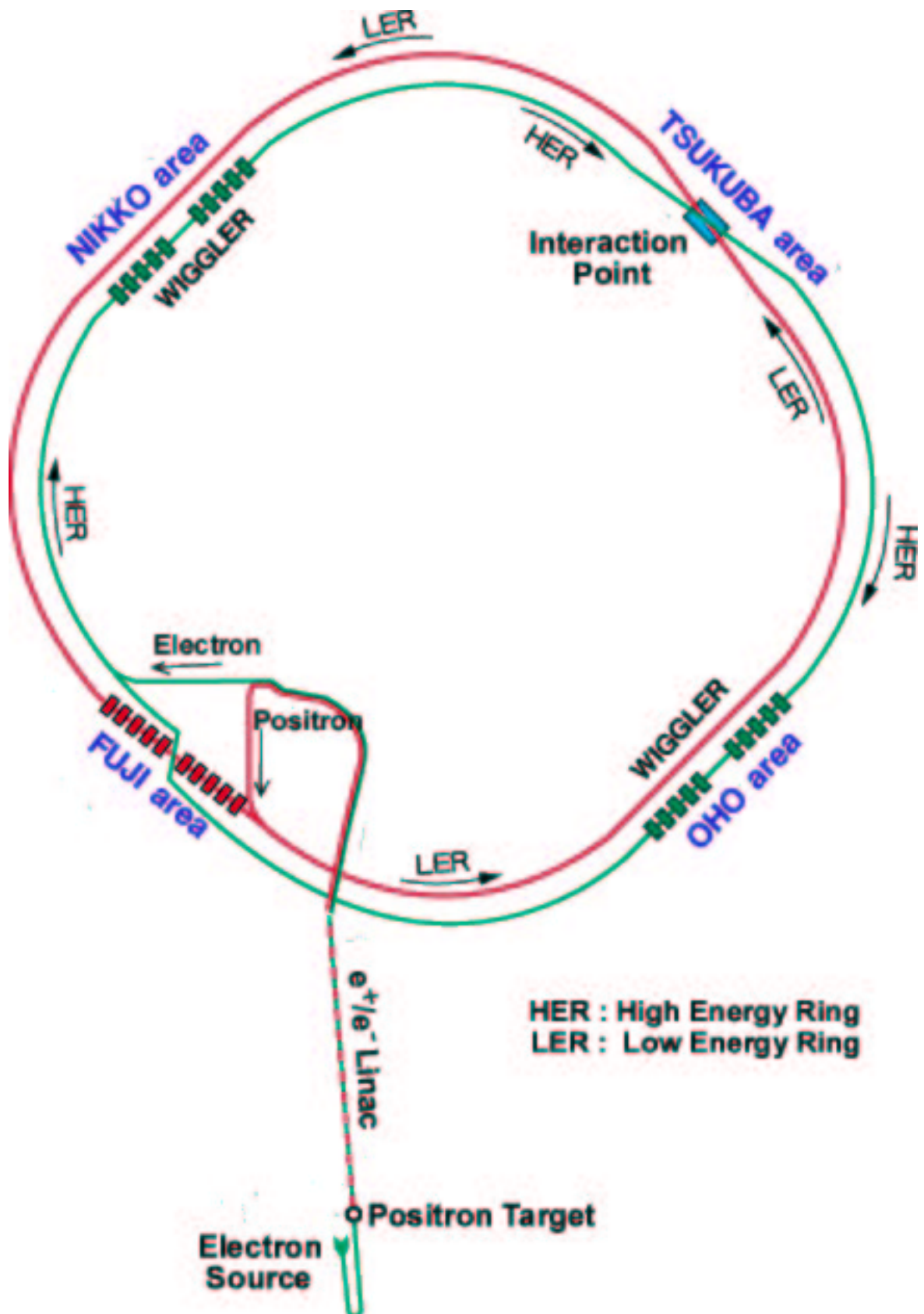


Figure 2.1: Configuration of the KEKB storage ring.



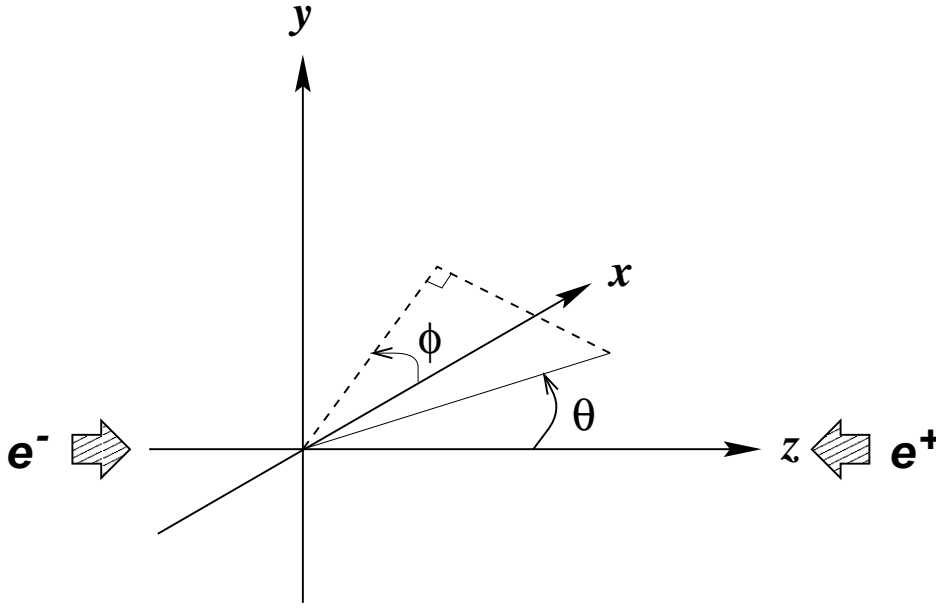


Figure 2.3: Definition of Belle coordinate system.

description of the SVD and its performance is given in [5].

### 2.2.2 Central Drift Chamber (CDC)

The role of the CDC is to measure the track positions, momentum and specific ionization ( $dE/dx$ ) of charged particles. The  $dE/dx$  information is used for the particle identification, combined with other particle identification detectors (ACC/TOF). In addition, another indispensable role of the CDC is to provide an online hardware trigger (so called “Level 1 trigger”). So far, only the CDC can provide a trigger for particles which come from near the IP.

The CDC is a small-cell drift chamber containing 50 anode layers (32 axial and 18 stereo wire layers) and 3 cathode strip layers. The anode layers are grouped into 11 superlayers (6 axial and 5 stereo superlayers). Combining axial and stereo hit information, 3-dimensional track reconstruction becomes possible. The cathode layers are located at the inner most part of the CDC, which measure the  $z$  position of a charged tracks. The number of readout channels is 8400 for anodes and 1792 for cathode in total. Figure 2.5 shows the geometrical configuration of the CDC. The CDC covers the region of 77 mm to 880 mm in radius and  $17^\circ$  to  $150^\circ$  in polar angle. Low Z-gas(50% He and 50%  $C_2H_6$ ) is used to reduce multiple scattering of a

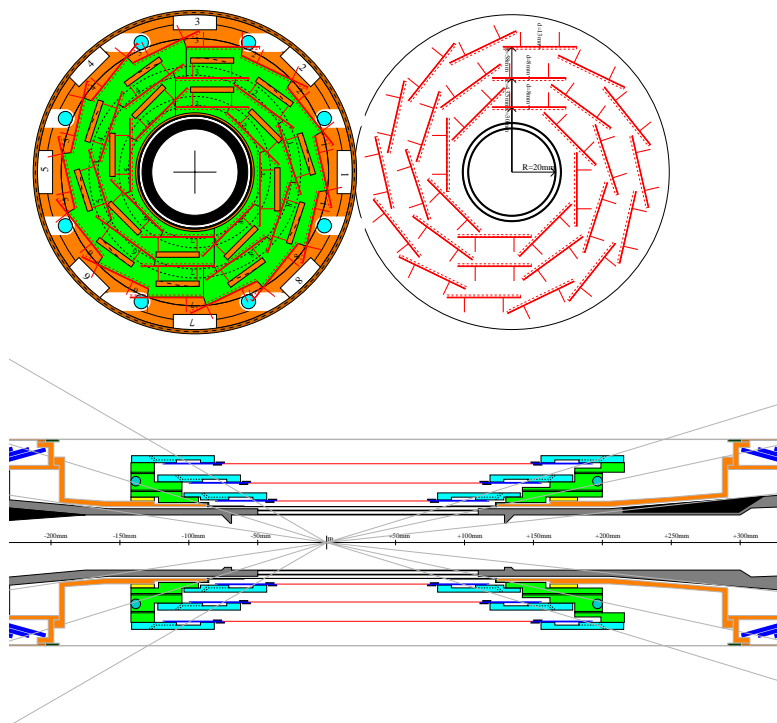


Figure 2.4: Silicon vertex detector.

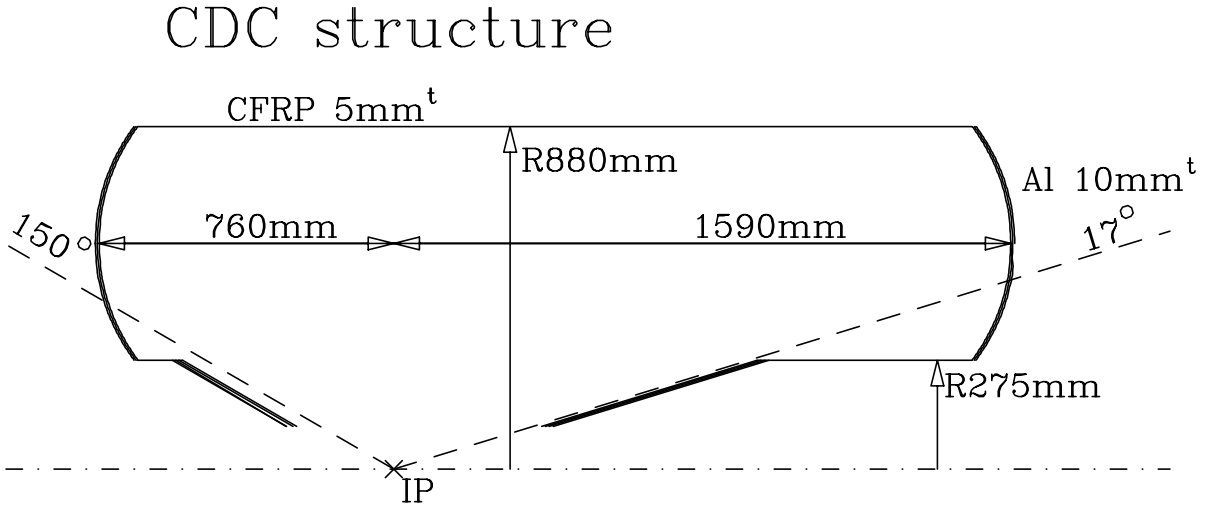


Figure 2.5: Central drift chamber.

charged particles. In spite of low  $Z$ -gas, a good  $dE/dx$  resolution is obtained owing to a large content of ethane.

The spatial resolution is  $130 \mu\text{m}$  in  $r - \phi$  plane and less than  $2 \text{ mm}$  in  $z$ , which leads the transverse momentum resolution  $\sigma_{p_t}/p_t$  of  $\sqrt{(0.19p_t)^2 + 0.34^2}\%$  where  $p_t$  is the transverse momentum in  $\text{GeV}/c$ . The  $dE/dx$  resolution is  $6.9\%$  for minimum ionizing particles. A more detailed description is given in [6].

### 2.2.3 Aerogel Čerenkov Counter (ACC)

The ACC provides an information to separate charged kaons from charged pions in high momentum range ( $1.2 \text{ GeV}/c < p < 3.5 \text{ GeV}/c$ ), which extend the reach of TOF. The ACC is an array of threshold type silica aerogel Čerenkov counters. It consists of two part; barrel and endcap.

The barrel part consists of 960 aerogel counters that are segmented into 16 division in  $z$  and 60 in  $\phi$ . The aerogel refractive index varies with the polar angle ( $n = 1.01, 1.013, 1.015, 1.020$  and  $1.028$ ) and has been optimized to match the kinematics of two-body decays from the boosted  $B$  mesons. Figure 2.6 shows the configuration of barrel ACC. The Čerenkov light from each barrel counter is fed into one or two fine-mesh photo-multipliers (FM-PMT) which can work in the  $1.5 \text{ T}$  magnetic field through air lightguides. The number of readout channels for the barrel ACC is 1560 in total.

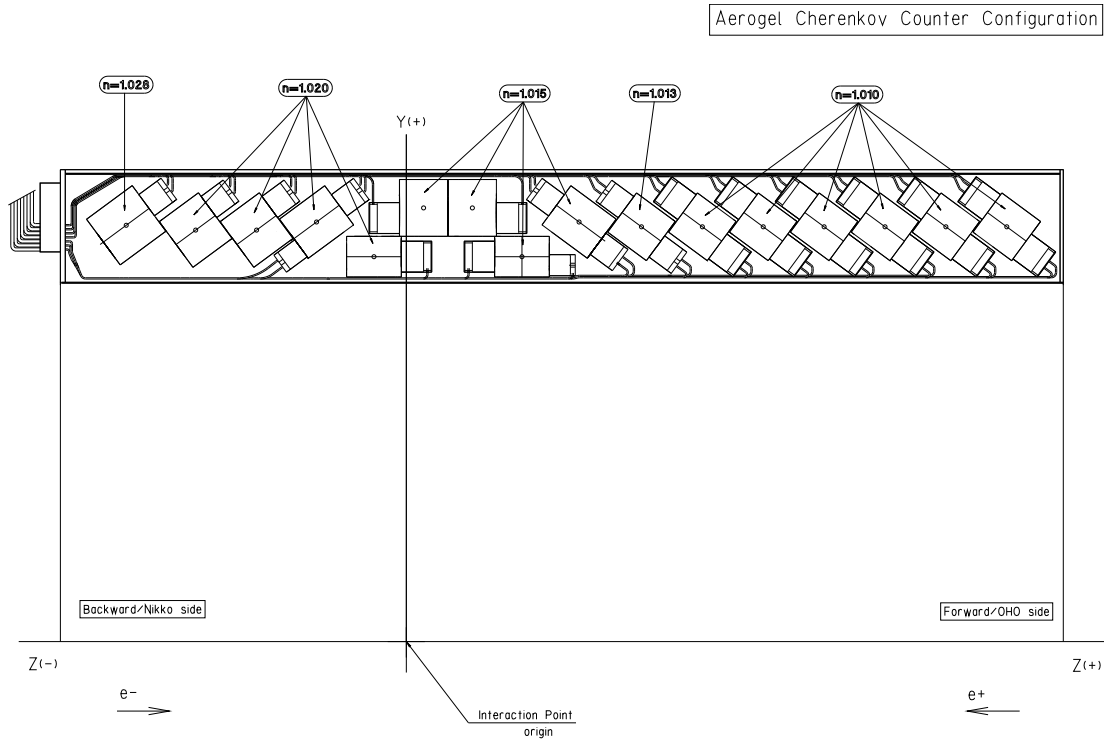


Figure 2.6: Barrel aerogel Čerenkov counter.

The endcap ACC is placed only in the forward side. It consists of 228 counters with  $n = 1.03$ . The counters are mounted in five concentric rings with different radii. Each ring contains 36, 36, 48, 48 and 60 counters from inner to outer. Each endcap counter has one FM-PMT for readout and therefore the number of readout channels is 228. Figure 2.7 shows the configuration of endcap ACC. A more detailed description of the ACC and its performance is given in [7].

#### 2.2.4 Trigger/Time of Flight counter (TSC/TOF)

The TOF is used to distinguish charged kaons from charged pions in the low momentum region ( $p < 1.2 \text{ GeV}/c$ ). The Trigger Scintillation Counter (TSC) together with the TOF generates the primary timing signal for the Level 1 trigger.

The configuration of TOF/TSC module is shown in Figure 2.8. Two trapezoidally shaped 4 cm-thick TOF scintillators and one 0.5 cm-thick plate TSC scintillator form one module. In total 64 modules are placed at 1.2 m from IP and cover  $34^\circ < \theta < 120^\circ$ . TOF information is read out by FM-PMTs at both ends of scintil-

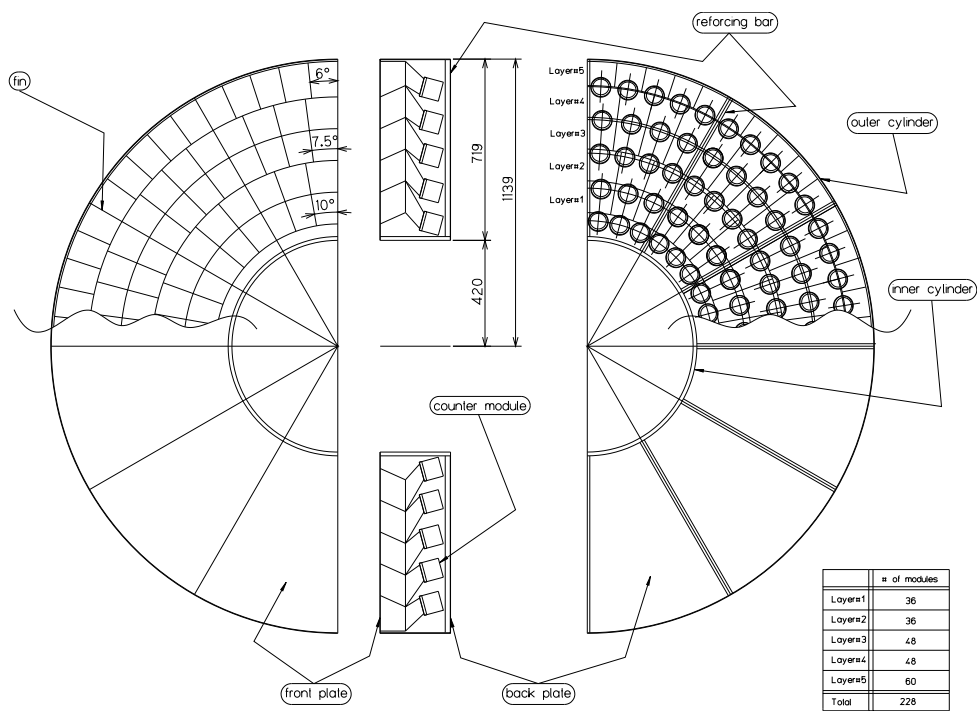


Figure 2.7: Endcap aerogel Čerenkov counter.

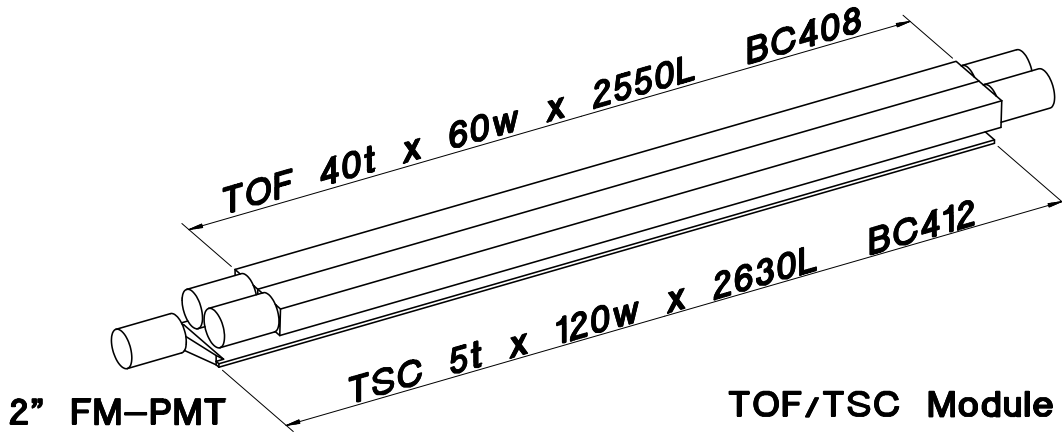


Figure 2.8: Time of flight and trigger scintillator counters.

lators, while TSC is read out by single FM-PMT from the backward end. The total number of readout channels of TOF is 320. The detail of the TOF is given in [8].

### 2.2.5 Electromagnetic Calorimeter(ECL)

The ECL measures the energy deposit of particles using the scintillation light from electromagnetic shower which charged and neutral particles generate in the CsI(Tl) crystals. Photons deposit most of their energy in the crystals, thus we can measure the energy of the photons. Electrons also deposit large energy that we can consider the tracks which has good agreement with ECL hits are electron. The ECL provides various triggers and also provides the secondary timing signal for the L1 trigger. Figure 2.9 shows the configuration of the ECL. The ECL consists of total 8736 CsI(Tl) crystals. the barrel part is installed radii is 125 cm from IP and covers the polar angle region of  $32.2^\circ < \theta < 128.7^\circ$ . The forward and backward endcap ECL is placed at  $z = 196$  cm and  $-102$  cm and covers  $12.01^\circ < \theta < 31.36^\circ$  and  $131.5^\circ < \theta < 155.0^\circ$  respectively. The 6624, 1152 and 960 crystals with two  $2\text{ cm} \times 1\text{ cm}$  photodiodes for read out are filled in barrel, endcap forward and endcap backward modules respectively.

The energy resolution measured by a photon beam test with the threshold energy of 0.5 MeV and with the  $5 \times 5$  crystal matrix is  $\sigma_E/E = 0.066\%/E \oplus 0.81\%/E^{1/4} \oplus 1.34\%$  and the position resolution is  $\sigma_{pos} = 0.5\text{ cm}/\sqrt{E}$ , with the unit of  $E$  in GeV. The detail of the ECL is given in [9].

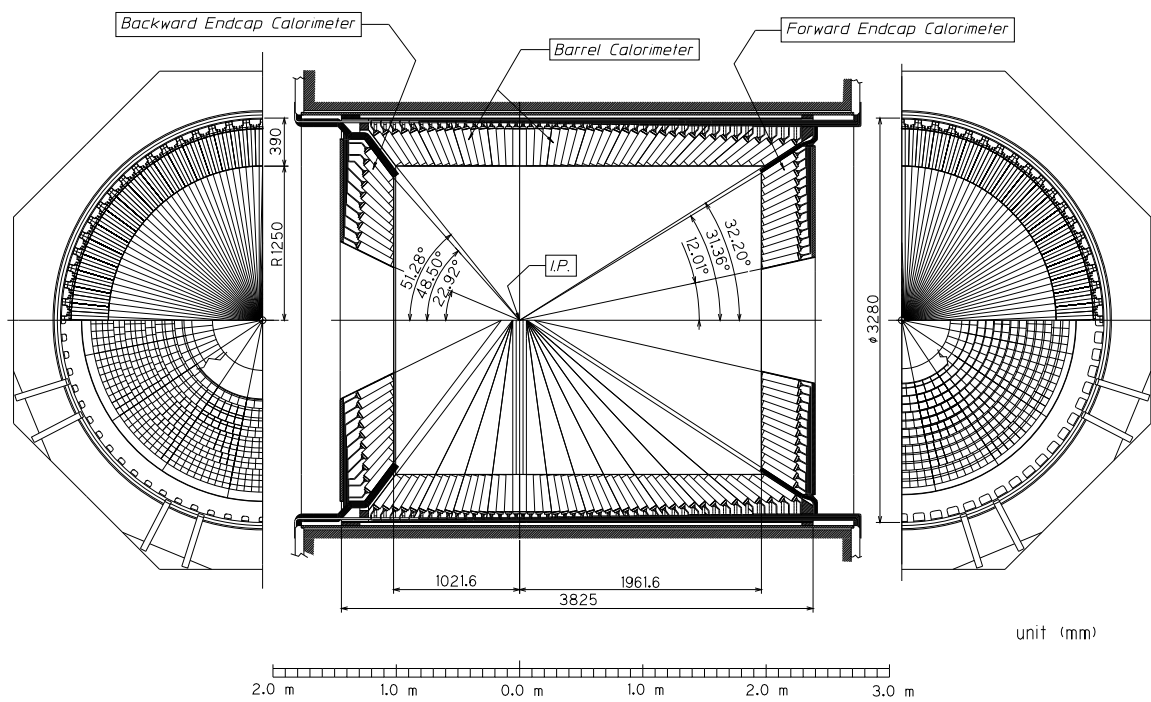


Figure 2.9: Electromagnetic calorimeter

### 2.2.6 $K_L/\mu$ detector (KLM)

The KLM detector is designed to identify the  $K_L$  mesons and muons over a broad momentum range above 600 MeV/c. The KLM consists of alternating layers of glass resistive plate counter (RPC) filled up with the gas mixture (30 % argon, 8 % butane and 62 % HFC134a) and 4.7 cm-thick iron plates. The high voltage is applied to the glass plate electrodes. When charged particles go through the ionize gas in the RPC, the amplified signals is picked up by the strips sticked outer side of glasses. The  $K_L$  mesons interact with iron and give a small hadron shower that we can detect. Muon lose energy only through ionization. On the other hands, hadrons interact strongly with the iron and scatter randomly usually without managing to penetrate more than a few KLM layers. Thus we can separate muon with hadrons. Figure 2.10 and 2.11 shows the configuration of the barrel and endcap KLM respectively. The KLM consists of an octagonal barrel detector and two endcap detectors that are divided into quadrant part of modules. The barrel modules are rectangular in shape and vary in size from  $220 \times 151$  to  $220 \times 267$  cm<sup>2</sup>. The endcap modules are in fan shape, and the inner radius is 130.5 cm, outer radius is 331 cm. The KLM covers the polar angular region of  $25^\circ < \theta < 145^\circ$ . The number of readout channels of KLM is 21856 in barrel and 16128 in endcap. From the cosmic ray measurement, we estimate the angular resolution of hit point from the IP is better than 10 mrad and the time resolution of KLM system is  $\sim$  several nsec. The detail of the KLM is given in [10].

### 2.2.7 Extreme Forward Calorimeter (EFC)

The EFC measures the energy of the photons and electrons at the extreme forward and backward direction out of the ECL acceptance. We use BGO ( $\text{Bi}_4\text{Ge}_3\text{O}_{12}$ ) crystals because the EFC is exposed in high irradiation (about 5 MRad/year) of photons from the synchrotron radiation and the spent electrons. EFC is installed attached to the front faces of the cryostats of the compensation solenoid magnets of the KEKB storage ring, surrounding the beam pipe as shown in the Figure 2.12. More detail of the EFC is described in [11].

### 2.2.8 Trigger and Data Acquisition system (DAQ)

#### Trigger system

In order to record the data of the physics events of our interest, we have to provide the common stop signal for TSC's and the gate signal for ADC's. Figure 2.13 shows the logic diagram of the trigger system. We combine sub-triggers from sub-detectors in what we called the Global Design Logic (GDL) and form the master triggers. A

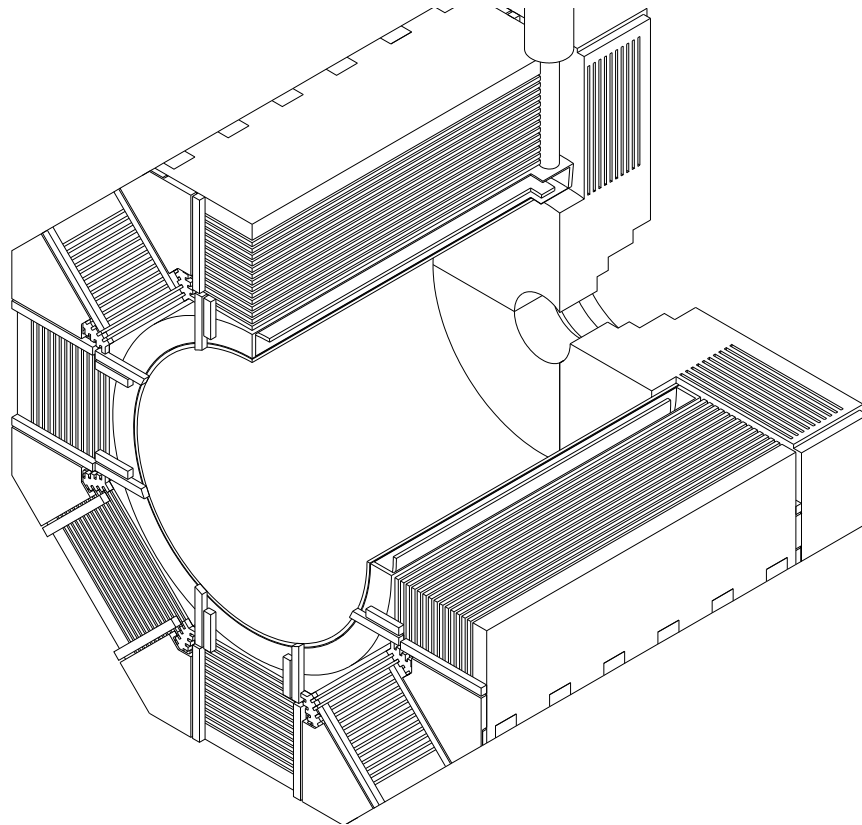


Figure 2.10: Schematic view of barrel KLM.

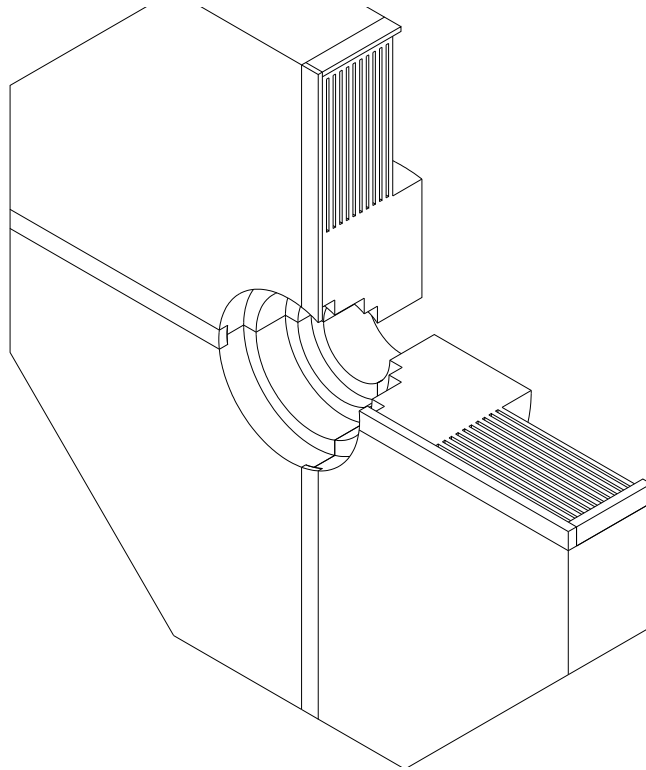


Figure 2.11: Schematic view of endcap KLM.

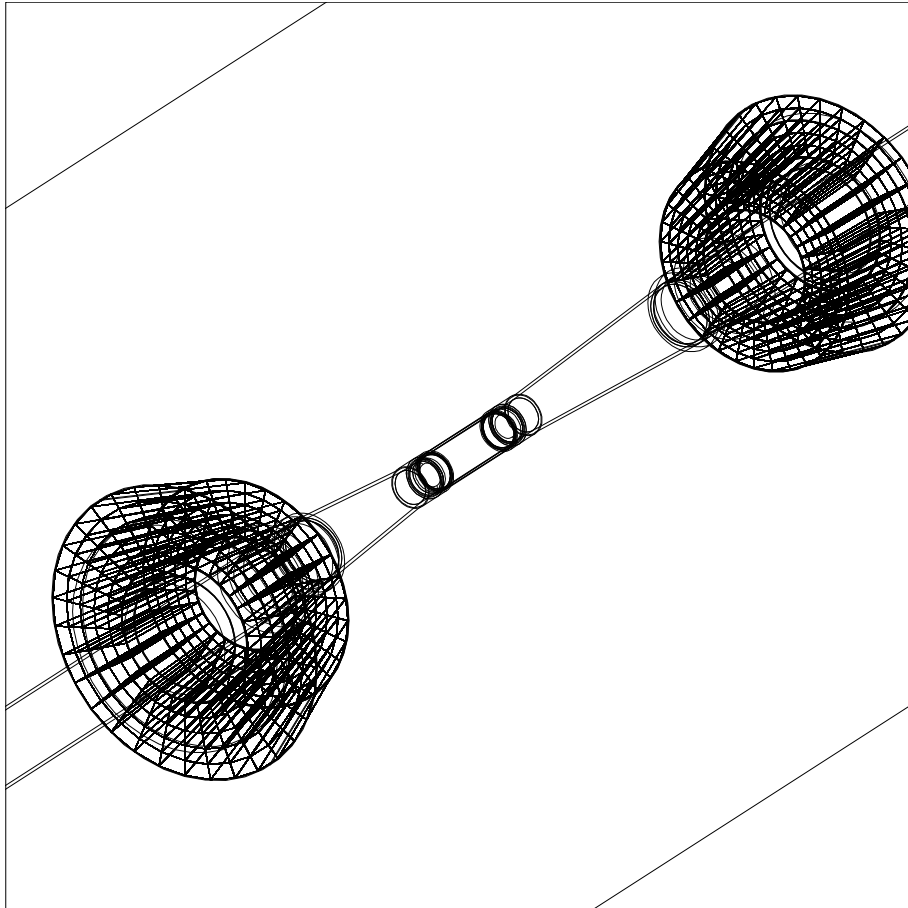


Figure 2.12: Extreme forward calorimeter.

decision for the triggers is made within  $2.2 \mu\text{s}$  after the beam collision at the IP. Typical trigger rate was 200 Hz, with which the DAQ deadtime is about 4 %.

### Data Acquisition system

In order to achieve the data acquisition with a deadtime fraction less than upto 500 Hz of trigger rate, a distributed-parallel DAQ system has been devised. A schematic view of the Belle data acquisition system is shown in Figure 2.14. The subsystem for readout from sub-detectors and also from the trigger systems run in parallel. We adopt a charge-to-time(Q-to-T) conversion frontend electronics, except for KLM which provides the time-multiplexed information on a signal line. The data from each subsystem are combined into single event recorded by the event builder which converts the “detector-by-detector” parallel data streams to “event-by-event” river. The event builder output is transferred to the online computer farm. The online farm consists of 120 processors for the fast reconstruction of up to 15 MBytes/sec event data stream. After passing the computer farm, the events are stored into the mass storage system and eventually stored into the tapes for off-line use.

## 2.3 Software

We give a brief overview of the structure of the analysis environment and the description of Monte Carlo simulation program optimized to the Belle experiment.

### 2.3.1 Overview

The raw data taken by the DAQ are processed in off-line using several kinds of reconstruction tools. The hits in the SVD and CDC are associated by the charged particle tracker. The energy management converts the information from ECL to the energy and flight direction of photons. The particle identification (PID) tools provide the information about the kind of the particles. These information from reconstruction tools are stored into Data Summary Tape (DST). For the physics analysis, DSTs are so large that we convert it more convenient and compact subset of data (Mini-DST).

To manage MDSTs and get the final result, analysis and simulation tools consist of many program modules which are executed on a common framework so called “BASF”.

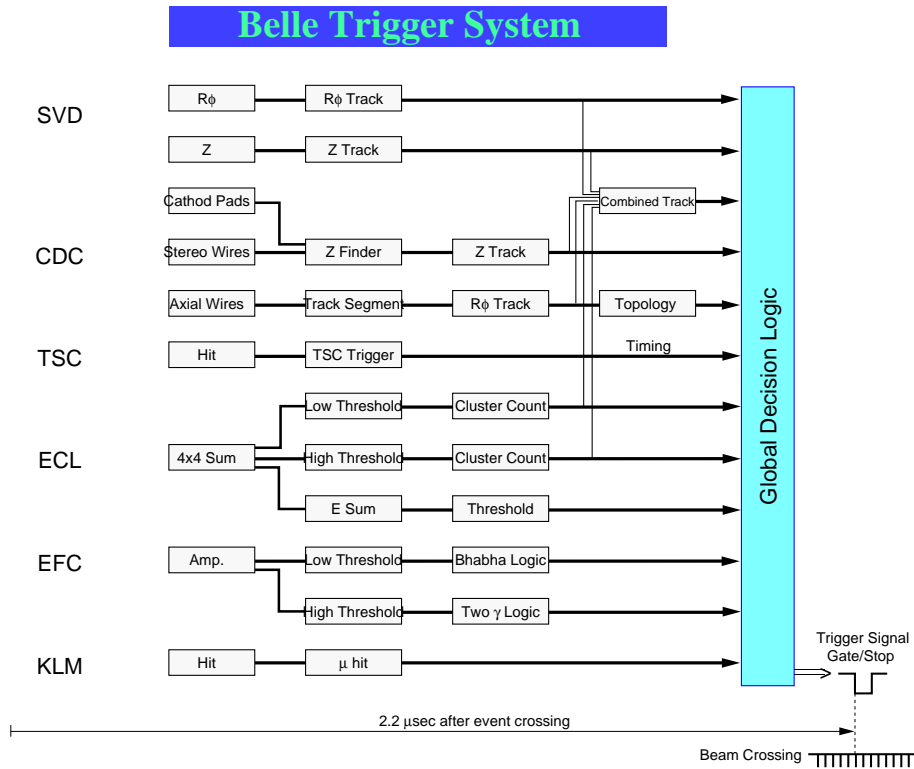


Figure 2.13: Logic diagram of Belle trigger system

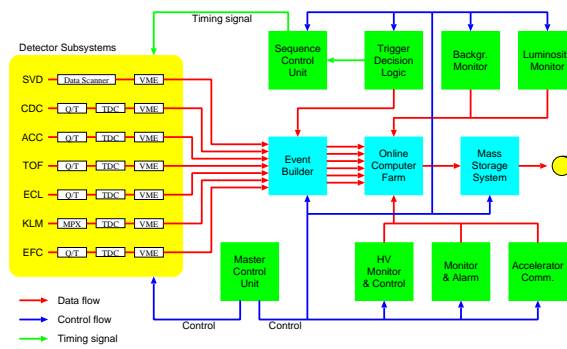


Figure 2.14: Logic diagram of Belle Data Acquisition system

### 2.3.2 Monte Carlo simulator

For Monte Carlo simulation, we have two detector simulator. One is the fast simulator and another is the full detector simulator. The fast simulator (FSIM) uses the parameterized detector performance, and generate MDST data directly. The FSIM does not need so much CPU power, but can not simulate detailed environment as to the detector resolution and so on. It was great advantage of CPU power is occurred in recent years, we can simulate enormous number of interaction between the particle from the event and our detector. We use GEANT [12] based full detector simulator (GSIM) in this analysis. When we input the event, the GSIM generates detector response. Data generated by GSIM is processed by the reconstruction tools, and subsequent process is the same as real data. For Monte Carlo event generation, we use three kind of generators. For  $\tau$  pair event generation, KORALB [13] event generator is used. The KORALB was developed for the  $\tau$  pair production process at low energies,  $\sqrt{s} < 30$  GeV. We use on the other hands QQ [14] event generator for background hadronic event ( $B\bar{B}$  and  $q\bar{q}$  for continuum). The QQ was developed for study of  $B$  mesons in the  $\Upsilon(4S)$  resonance. Both of generators are developed by CLEO [?] collaboration so that designed for a symmetric collider, they have been adjusted to describe the Belle experiment. Also for the background estimation, we use aafhb generator ?? for the two photon process. The aafhb is the modified aafh generator for BELLE. The aafh calculates the four-fermion production from  $e^+e^-$  collisions. The decay table that is control the decay of generated particle is described according to latest Particle Data Group (PDG) [16] value, also we can be modified and define the interactions and the final products. We generate Monte Carlo of  $\tau \rightarrow \ell K^0$  events (signal events) using KORALB and modified decay table in assumption of the angular distribution of the  $\tau$  decay to the signal is uniform in the rest system of  $\tau$ .

# Chapter 3

## Analysis

### 3.1 Lifetime measurement method

In this analysis, we determine the tau lifetime by using “decay length method”. In this method, we calculate the decay length ( $L$ ) between interaction point (IP) and vertex formed by the 3-prong tau decay tracks, and measure the mean of their distribution. We use a sample of 1-3 topology  $\tau$ -pair event. Branching fraction of 1-prong decay and 3-prong decay is

$$\begin{aligned} B(\tau \rightarrow 1 - prong) &= (85.35 \pm 0.07)\% \\ B(\tau \rightarrow 3 - prong) &= (14.57 \pm 0.07)\% \end{aligned}$$

About 25% of all  $\tau$ -pair event decay into 1-3 topology.

#### 3.1.1 Proper Decay Length

By measuring mean decay length, the tau proper decay length,  $c\tau$ , is calculated from

$$c\tau = \frac{L}{\gamma\beta} = \frac{m_\tau}{p_\tau} \frac{L_{xy}}{\sin\theta} \quad (3.1)$$

where  $L$ ,  $p_\tau$ ,  $m_\tau$  and  $\theta$  are the decay length of tau, the magnitude of the tau’s momentum, the world average value of the tau mass (1777MeV) and the polar angle of tau momentum direction. We determine the magnitude of the tau momentum,  $p_\tau$  from the beam energy and polar angle of the reconstructed tau particle.  $L_{xy}$  is the component of the flight path in the precision measurement projection, transverse to the  $z$  axis. We determine the  $\theta$  from the combined vector momentum of the three charged tracks.

Shown in Figure 3.1 (b) is the difference between generated decay length  $L_{gen}$  and reconstructed decay length,  $L$  using a Monte Carlo simulation (Figure 3.1)

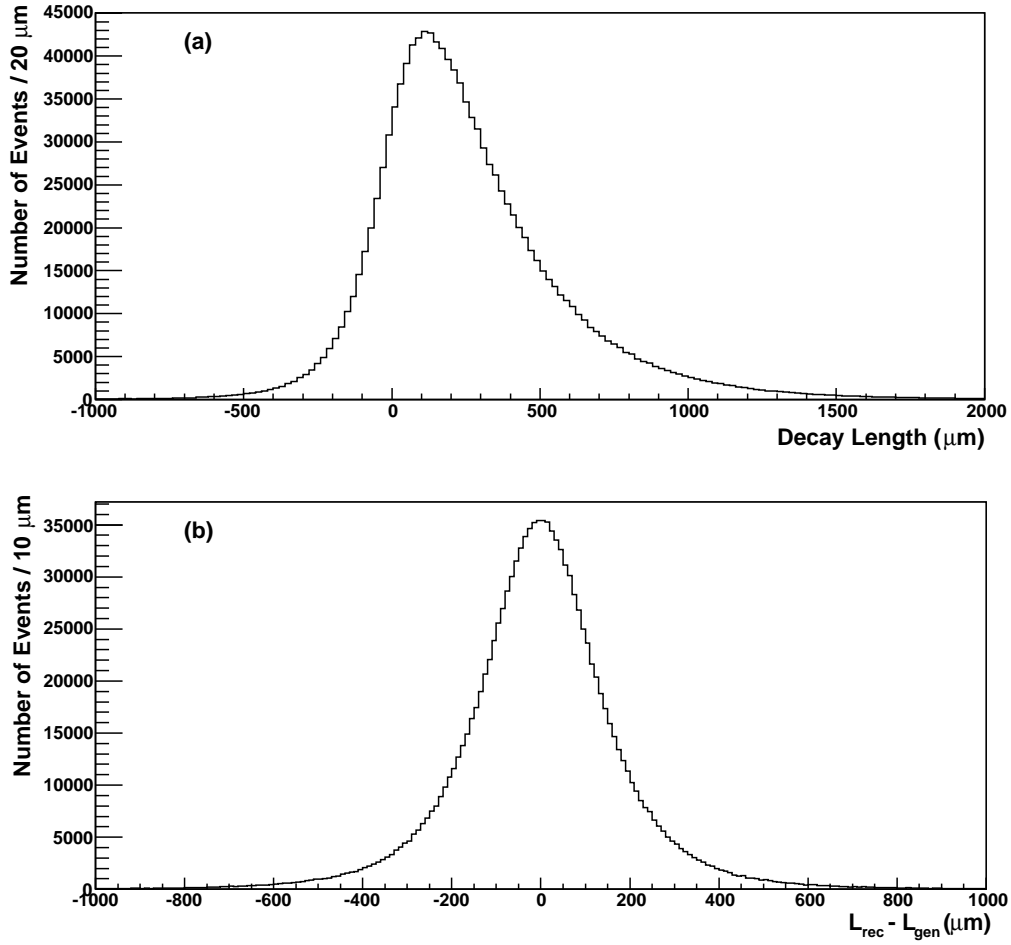
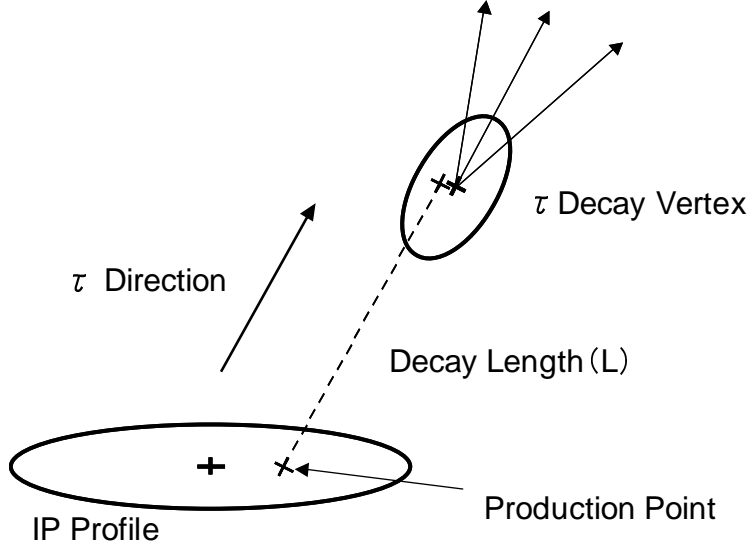


Figure 3.1: (a) The reconstructed decay length of tau-pair MC,  $L$  (b) Difference between the reconstructed decay length,  $L_{rec}$  and generated decay length,  $L_{gen}$  of MC

### The momentum of tau

Because of missing neutrino, we cannot measure the tau's momentum. We compute the magnitude of the momentum using beam energy and tau's direction,  $\theta$ . We assume tau's direction,  $\theta$  is equal to the direction of combined momentum vector of charged tracks in 3-prong side.

Figure 3.2: Schematic view of the  $\tau$  vertex

### 3.1.2 Decay Length Reconstruction

The tau lepton lifetime is measured using two dimensional distance between the decay vertex and production vertex of reconstructed tau lepton. Figure 3.2 shows the reconstruction of decay length. The decay vertex of reconstructed tau lepton is obtained using 3-prong charged tracks. The production point is estimated from Interaction Point(IP).

The projected decay length  $L_{xy}$  is calculated by

$$L_{xy} = \frac{Xt_x\sigma_y^2 + Yt_y\sigma_x^2 - (Xt_y + Yt_x)\sigma_{xy}}{t_y^2\sigma_x^2 + t_x^2\sigma_y^2 - 2t_xt_y\sigma_{xy}} \quad (3.2)$$

with  $X = X_v - X_b$ ,  $Y = Y_v - Y_b$ . In the equation,  $(X_v, Y_v)$  are decay coordinates of  $\tau$  decay point.  $(X_b, Y_b)$  are the interaction point.  $(\sigma_x^2, \sigma_y^2, \sigma_{xy})$  are error matrix components formed by adding the error matrices for the IP and the decay vertex.  $t_x$  and  $t_y$  are two dimensional direction cosines of the three-prong momentum vector. This direction is approximation to the flight direction of  $\tau$ .

### 3.1.3 Measuring the mean lifetime

We determine the lifetime using average of proper decay length distribution.

The probability that unstable particle decays at time  $t'$  is  $(1/\tau)e^{-t'/\tau}$ . The mean

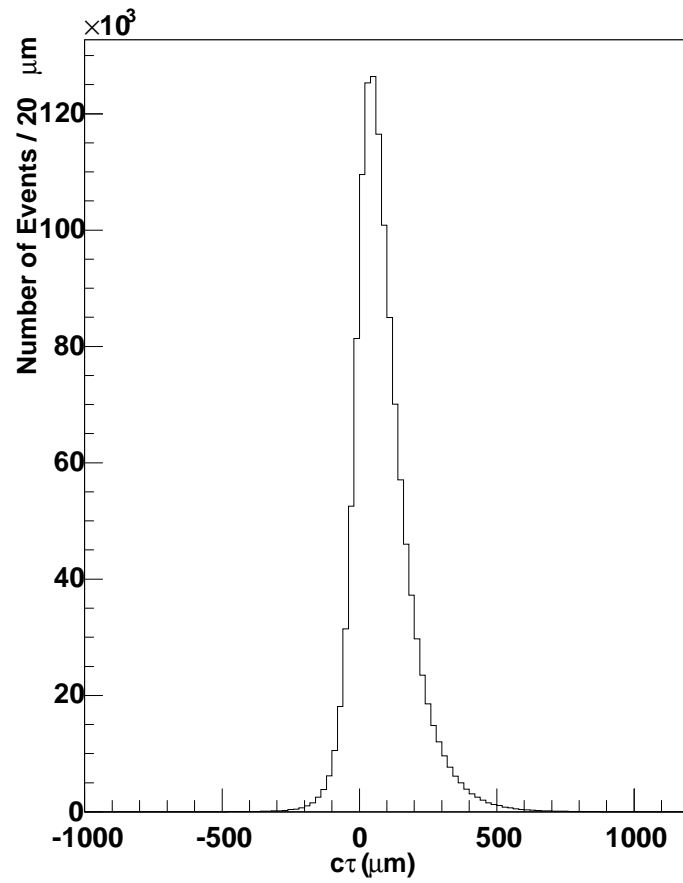


Figure 3.3: Proper decay length  $c\tau$  of  $\tau$ -pair MC.  $\langle c\tau \rangle = (83.97 \pm 0.09)\mu\text{m}$

lifetime of this particle is

$$\begin{aligned}
 \langle \tau \rangle &= \int_0^{\infty} t' P(t') dt' \\
 &= \frac{1}{\tau} \int_0^{\infty} t' e^{-t'/\tau} dt' \\
 &= \tau
 \end{aligned} \tag{3.3}$$

In the experiment, the observed decay distribution is not an exponential, because of the limited detector accuracy. The shape of the distribution is an exponential distribution convoluted with resolution smearing function,

$$\begin{aligned}
 \langle \tau \rangle &= \int_{-\infty}^{\infty} t' P(t, t') dt' \\
 &= \frac{1}{\tau} \int_{-\infty}^{\infty} \left( \int_0^{\infty} e^{-t/\tau} \sum_{i=1}^N t' f_i(t') dt \right) dt' \\
 &= \frac{1}{\tau} \int_0^{\infty} e^{-t/\tau} \left( \sum_{i=1}^N \int_{-\infty}^{\infty} t' f_i(t') dt \right) dt'
 \end{aligned} \tag{3.4}$$

where  $P(t, t')$  is the probability density function.  $f_i(t')$  are smearing function which are centered at  $t'$ . If we assume that the smearing function are a set of Gaussian, Equation 3.4 becomes,

$$\begin{aligned}
 \langle t \rangle &= \int_{-\infty}^{\infty} t' \left( \int_0^{\infty} \frac{1}{\tau} e^{-t/\tau} \sum_{n=1}^N \frac{1}{\sqrt{2\pi}\sigma_i} e^{-\frac{(t'-t)^2}{2\sigma_i^2}} dt \right) dt' \\
 &= \frac{1}{\tau} \int_0^{\infty} e^{-t/\tau} \left( \sum_{n=1}^N \frac{1}{\sqrt{2\pi}\sigma_i} \int_{-\infty}^{\infty} t' e^{-\frac{(t'-t)^2}{2\sigma_i^2}} dt' \right) dt \\
 &= \frac{1}{\tau} \int_0^{\infty} t e^{-t/\tau} dt \\
 &= \tau
 \end{aligned} \tag{3.5}$$

Equation 3.5 says that the mean of exponential distribution is preserved when smearing function is Gaussian.

### 3.1.4 Calculating the lifetime

The relation between the  $\tau$  mean lifetime,  $\tau_{\tau}$  and the mean lifetime of the event sample,  $\tau_m$  is

$$\tau_m = f_\tau \alpha \tau_\tau + f_{bg} \tau_{bg} \quad (3.6)$$

with

$$f_\tau + f_{bg} = 1 \quad (3.7)$$

where  $f_\tau$  is the fraction of tau,  $f_{bg}$  is background fraction,  $\tau_{bg}$  is the mean lifetime of background and  $\alpha$  is a correction factor including the initial state radiation. We calculate  $\alpha$  using Monte Carlo. This correction is described in section 3.6.

We can obtain the tau lifetime,  $\tau_\tau$  from Equation 3.6

$$\begin{aligned} \tau_\tau &= \frac{\tau_m - f_{bg} \tau_{bg}}{f_\tau \alpha} \\ &= \frac{\tau_m - f_{bg} \tau_{bg}}{(1 - f_{bg}) \alpha} \end{aligned} \quad (3.8)$$

The statistical error on the tau lifetime is the derivative of equation (3.8)

$$\begin{aligned} \sigma_{\tau_\tau}^2 &= \frac{1}{\alpha^2} \frac{1}{(1 - f_b)^2} \sigma_{\tau_m}^2 + \frac{1}{\alpha^2} \frac{1}{(1 - f_b)^2} f_b^2 \sigma_{\tau_b}^2 \\ &\quad + \frac{1}{\alpha^2} \left[ \frac{\tau_m - \tau_b}{(1 - f_b)^2} \right]^2 \sigma_{f_b}^2 + \frac{1}{\alpha^4} \left[ \frac{\tau_m - f_b \tau_b}{1 - f_b} \right]^2 \sigma_\alpha^2 \end{aligned} \quad (3.9)$$

We determine  $\sigma_{\tau_b}$ ,  $\sigma_{f_b}$  and  $\sigma_\alpha$  by using Monte Carlo simulation.

## 3.2 The data set

This analysis is performed on data from BELLE experiment. For the lifetime measurements, we use Exp07 - Exp23 data set whose integrated luminosity is  $98.9 fb^{-1}$ . It corresponds to 89 million  $\tau$ -pair events assuming the cross section  $\sigma_\tau = 0.9 nb$ . A large part of the data is taken under the condition of the total beam energy  $W = 10.58 GeV$  to be in region of  $\Upsilon(4S)$  resonance. Some part of the data is taken at the energy  $30 \sim 60 MeV$  below the  $\Upsilon(4S)$  resonance, for the background study of  $B$ -physics. We call former as “on-resonance” data and later as “off-resonance” data. The cross section of  $\tau$  pair creation dose not change both of the condition, so we treat the off-resonance data as same as on resonance data.

For signal event study, we use 170 million  $\tau$ -pairs MC which decay into  $\tau \rightarrow$  generic mode.

For background study, we use Monte Carlo events of generic 123 million  $B\bar{B}$ , 245 million generic  $uds$  (combination  $u\bar{u}, d\bar{d}, s\bar{s}$ ), 152 million generic  $c\bar{c}$ .

## 3.3 Event selection

The selection criteria are listed in Table 3.1. After the all cut, we obtain 1349690 candidates of 1-3 topology tau decay event .

Table 3.1: List of Event selection

	requirement
	tau-skim topology
Event quality	SVD hits $> 1$ $\chi^2/n.d.f.$ of vertex fit $< 5$
BG rejection	$P_T^* > 2.0 GeV$ $m^{3p} < 1.8 GeV$ $M(e^+e^-) > 0.1 GeV/c^2$ $\theta_{miss} > 25^\circ$ Average opening angle $< 60^\circ$ lepton tag

### 3.3.1 $\tau$ pair event selection

We use the event through the  $\tau$ -pair skim. These are the tau pair event selection criteria we used generally at BELLE. This selection condition is optimized to suppress Bhabha,  $\mu$ -pair and two-photon event.

- $2 \leq \text{No. of good tracks} \leq 8$
- $\Sigma P^* < 10 \text{ GeV}/c$
- $\Sigma E(\text{ECL}) < 10 \text{ GeV}$
- $|\Sigma(\text{charge})| \leq 2$
- $P_{t\max} > 0.5 \text{ GeV}/c$
- $E_{rec}^* > 3 \text{ GeV}$  or  $P_{t\max} > 1 \text{ GeV}/c$
- $E_{tot}^* < 9 \text{ GeV}$  or  $\theta_{max} > 175^\circ$
- No. of tracks in barrel region  $\geq 2$  or  $E(\text{ECL}_{trk}) < 5.3 \text{ GeV}$
- $\theta_{max} > 20^\circ$

where

- \* denotes a center of mass (CM) system of  $e^+e^-$  collision,
- “ $\Sigma$ ” represents for the summation in an event,
- $X_{max}$  represents for maximum value of X in an event.
- Pt: transverse momentum,
- good charged track:  $P_t \geq 0.1 \text{ GeV}/c$ , helix  $|dr| < 3 \text{ cm}$ ,  $|dz| < 5 \text{ cm}$ ,
- $E_{rec}^*$ : Summation of momentum of all charged tracks and Energies of all gamma,
- $E_{tot}^*$ : Summation of  $E_{rec}^*$  and magnitude of the missing momentum,
- $E(\text{ECL}_{trk})$ : Summation of the energy of ECL hits without gamma.

### 3.3.2 Event Topology

The event topology is determined by defining a plane perpendicular to the thrust axis that is calculated by all charged track. We select 4 charged track event with zero net charge. And we divide the these tracks in two hemisphere. We require one hemisphere has three charged tracks (we call this hemisphere 'signal side') and other side has one charged track(tag side). Absolute value of net charge in both side is required to be 1.

### 3.3.3 Event quality

The charged tracks that are used to find a vertex must be associated with at least two SVD hits in both the  $r\phi$  and the  $rz$  planes. Figure 3.4 indicates the difference between the reconstructed and generated decay length ( $L_{xy}$ ),  $\Delta L$ .

The  $\chi^2/\text{ndf}$ (number of the degrees of freedom) of the vertex fit must be less than 5 to reduce poorly reconstructed events.

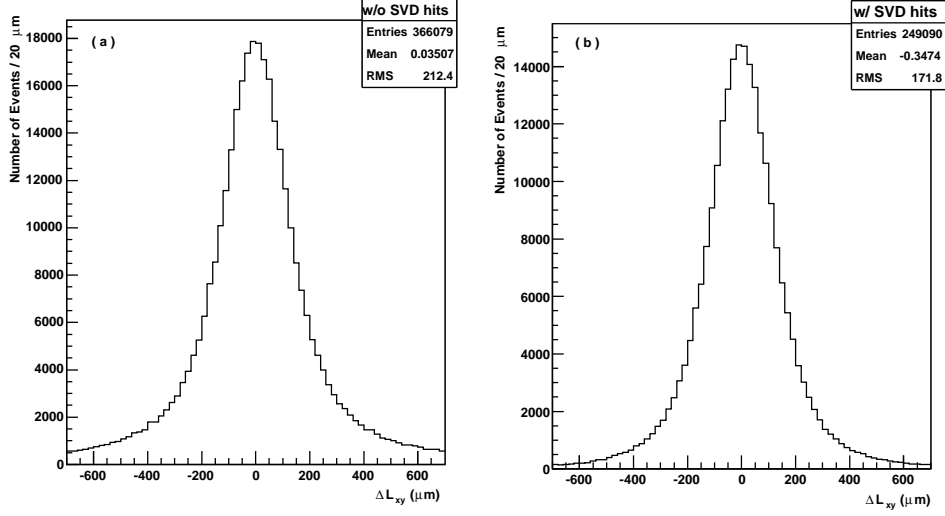


Figure 3.4: (a), (b) is  $\Delta L_{xy}$  distribution of Signal MC. (a) (b) is required SVD hits constraint. RMS becomes smaller, when we require the SVD hits constraint.

### 3.3.4 Background rejection

Shown in Figure 3.5 is a scatter plot on  $P_z^*$  vs  $P_T^*$ .  $P_T^*$  and  $P_z^*$  indicate the magnitude of transverse and z-axis component of total momentum vector of all 4-charged tracks in CMS. Two photon events have small total transverse momenta (figure 3.5 (c)).

We require the magnitude of transverse component of total momentum vector of all 4-charged tracks in CMS,  $p_T^*$  is larger than  $0.8 \text{ GeV}/c$ .

- $p_T^* > p_z^* - 1$  and  $p_T^* > -p_z^* - 1$
- $p_T^* > 0.8 \text{ GeV}/c$

To reject electrons from photon conversion, we require the invariant mass for all combination of opposite charged track, whose mass are assumed to be the electron,  $M(e^+e^-)$  is required to be larger than  $0.1 \text{ GeV}/c^2$ . Because  $e^+e^-$  pairs produced by photon conversion have total energy equal to the center of mass energy.

- $M(e^+e^-) > 0.1 \text{ GeV}/c^2$

The polar angle of missing momentum vector,  $\theta_{miss}$  should be in the detector acceptance. Because in Bhabha and two-photon event, charged track tend to fly along the beam direction.

- $\theta_{miss} > 25^\circ$

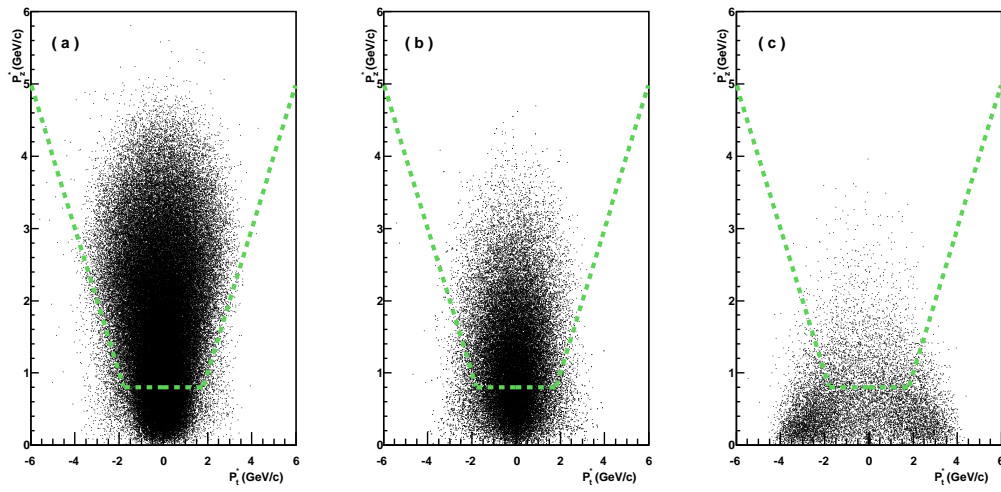


Figure 3.5: Scatter plots of  $P_T^*$  -vs-  $P_Z^*$  plane.(a)tau-pair MC, (b) $q\bar{q}$  continuum MC, (c)two-photon MC.

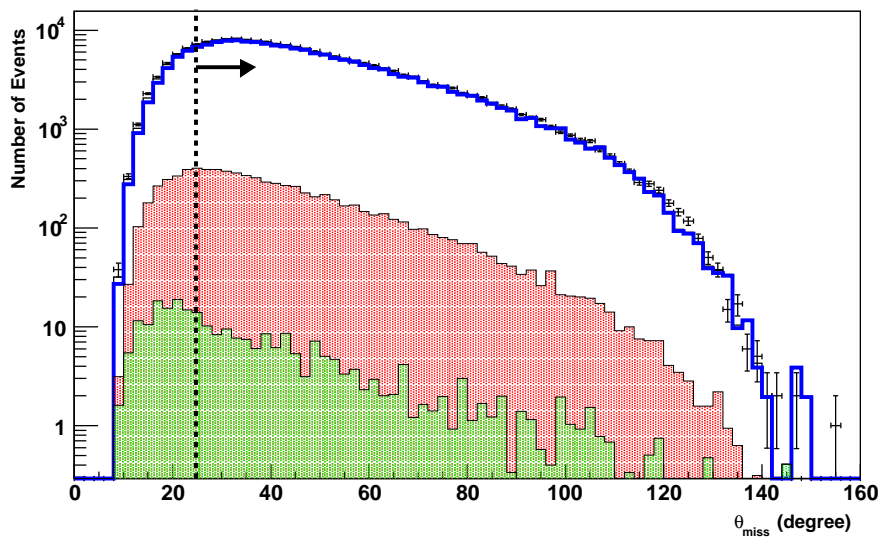


Figure 3.6: Angle of Missing momentum direction.Data are indicated by points with error bars.

To suppress hadronic background, we apply two selection criteria in their invariant mass and the average opening angle of three prong side. In the tau event, three-prong invariant masses,  $m^{3p}$  should be smaller than mass of tau particle( $1.777\text{GeV}$ ). So we require the cut criteria,  $m^{3p}$  less than  $1.8\text{ GeV}/c^2$ (figure3.7)

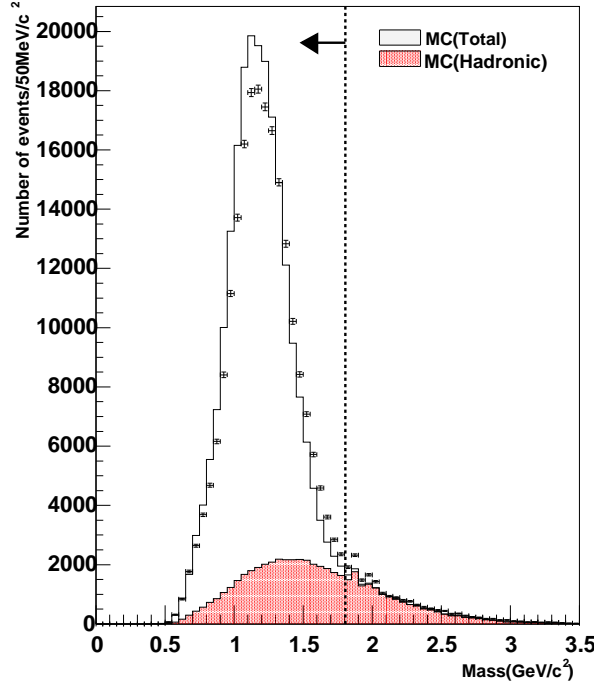


Figure 3.7: The invariant mass distribution of three prong side. Data are indicated by points with error bars.

The average opening angle means the average of three opening angles on three-prong side. Higher mass particles (like a hadronic events), have larger opening angle than tau daughters. Shown in figure 3.8 are the average opening angle distribution in CMS. Hadronic events produce decay products which have larger opening angles than those from tau daughter. we select events whose opening angle of 3-prong side is smaller than  $60^\circ$ .

- Invariant mass less than  $1.8\text{ GeV}/c^2$
- Average opening angle on the three prong side is smaller than  $60^\circ$

We request the particle of 1-prong side is lepton( $e$  or  $\mu$ ). This requirements reduce the many hadronic background events. The electron and muon are identified based on the particle identification software in BELLE.

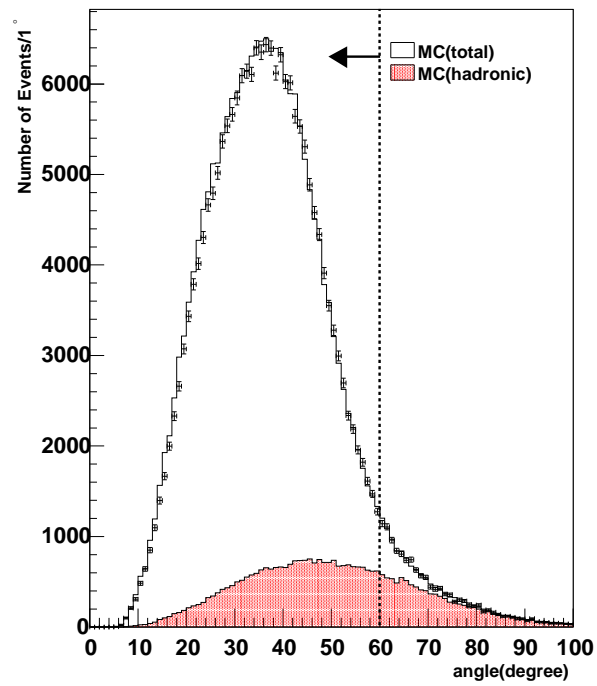


Figure 3.8: Average opening angle distribution. Data are indicated by points with error bars.

- We require the lepton in 1-prong side

Electrons is identified by requiring the ratio of energy deposited by the particle in the ECL to the momentum measured in the CDC is close to unity, and by using  $dE/dx$  information from the CDC and hits in the ACC.

Muon candidates are required to have a well reconstructed track in the muon system comprised of 12 layers of iron plate interleaved with KLM. Muon probability is calculated from two variables; one is the difference between the range calculated by the momentum of the particle and the range measured by KLM, and the other is the  $\chi$ -square of the KLM hits with respect to the extrapolated track.

The detail and general description of electron and muon identification system is the Belle is summarized in Ref [17][18]

### 3.4 A Comparison of data with Monte Carlo

To check the data quality, we compare our data set with Monte Carlo data set. We check reconstructed polar angle  $\theta$ , tau momentum  $p_\tau$ , and two-dimensional decay length  $L_{xy}$  in laboratory system. These values are used as input parameters in calculating the tau lifetime. Shown in Figure 3.9 and 3.10 indicate  $\theta$  and  $p_\tau$  distributions, respectively. These two values show good agreement with Monte Carlo data.

Shown in figure 3.11 indicates the two-dimensional decay length distribution. Decay length of data set has lager mean and R.M.S than that of Monte Carlo data set. Mean of experimental data set is  $209.95 \pm 0.23 \mu m$ , and Monte Carlo data is  $207.84 \pm 0.15 \mu m$ .

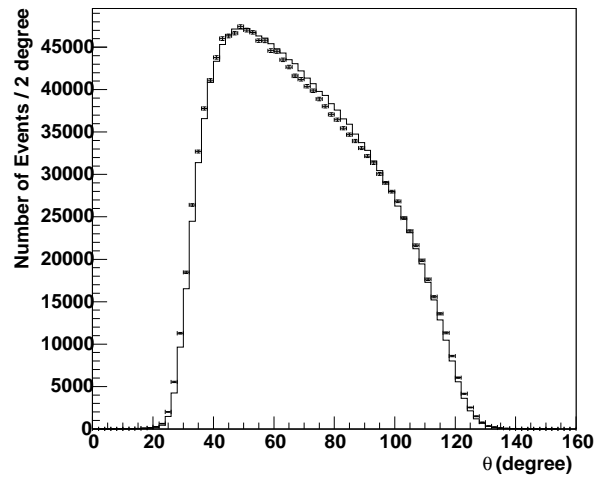


Figure 3.9: reconstructed theta distribution. Data are indicated by points with error bars, Monte Carlo by the solid histogram

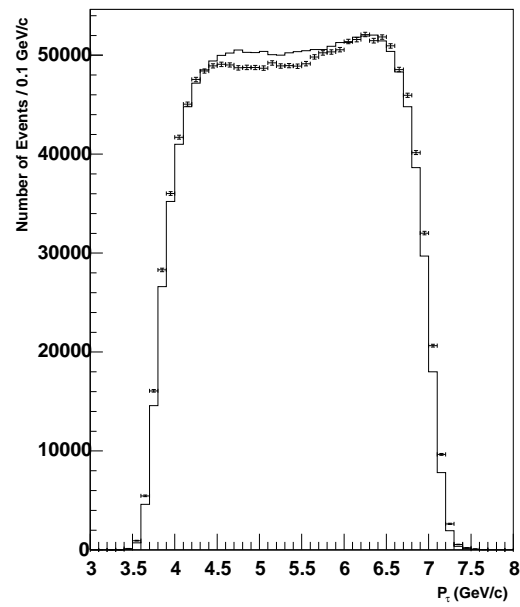


Figure 3.10: reconstructed tau distribution. Data are indicated by points with error bars, Monte Carlo by the solid histogram

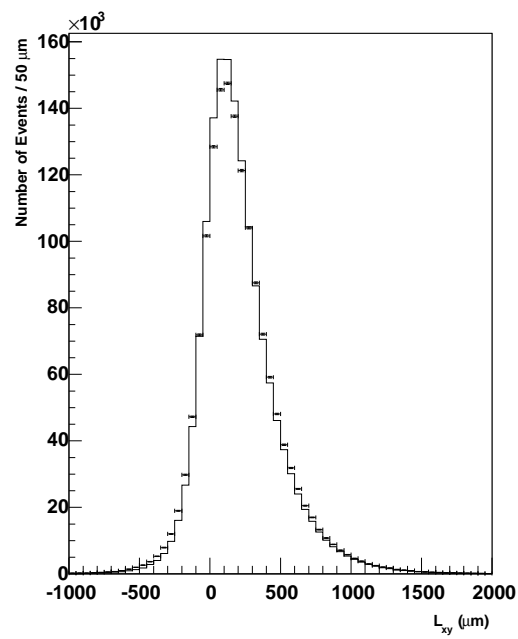


Figure 3.11: reconstructed two-dimensional decay length distribution. Data are indicated by points with error bars, Monte Carlo by the solid histogram

### 3.5 Estimate the Background event fraction

After all cuts, dominant backgrounds remaining in the sample are  $q\bar{q}$  continuum, and two photon events. We estimate these background fraction using Monte Carlo simulated events. We estimate the number of background event by counting the number of events passing the all cuts, and normalizing the Monte Carlo luminosity,  $\int L_{bg} dt$  to the integrated luminosity for the data set,  $\int L_{data} dt$ . The fraction of background is this number divided by the number of the 1 vs 3 events in the real data set. The background fraction,  $f_{bg}$  is defined as the following:

$$f_{bg} = \left[ N_{bg} \times \frac{\int L_{data}}{\int L_{bg}} \right] / N_m \quad (3.10)$$

$N_{bg}$  indicates the number of background events which through the all cuts.  $N_m$  is the number of candidates of the event sample. After the all cuts, 4.43% background events remain in the data set.

Shown in figure 3.12 is proper decay length distribution of background events using Monte Carlo sample. Background fraction and their proper decay length are listed in Table3.2

Table 3.2: Event fraction of background

	fraction(%)	$c\tau_{bg}(\mu m)$
$q\bar{q}$ continuum	4.34	$35.26 \pm 0.43$
two photon	0.09	$30.19 \pm 3.45$
<i>total</i>	$4.43 \pm 0.0001$	$35.16 \pm 0.46$

### 3.6 Correction

The reconstructed proper decay length ( $c\tau_m$ ) is shifted from the actual proper decay length, because of the initial state radiation and any other reconstruction bias . To correct the decay time, We estimate  $\alpha$  as the ratio of the reconstructed proper decay length,  $\tau_m$  to generated lifetime from Monte Carlo. The mean decay length of generated tau lepton,  $\tau_{gen}$  is  $87.11 \mu m$ . And reconstructed lifetime using  $\tau$ -pair Monte Carlo,  $\tau_{MC}$  is  $(84.37 \pm 0.09) \mu m$ .

We obtain the correction factor,

$$\alpha = \frac{\tau_{MC}}{\tau_{gen}} = (0.964 \pm 0.001). \quad (3.11)$$

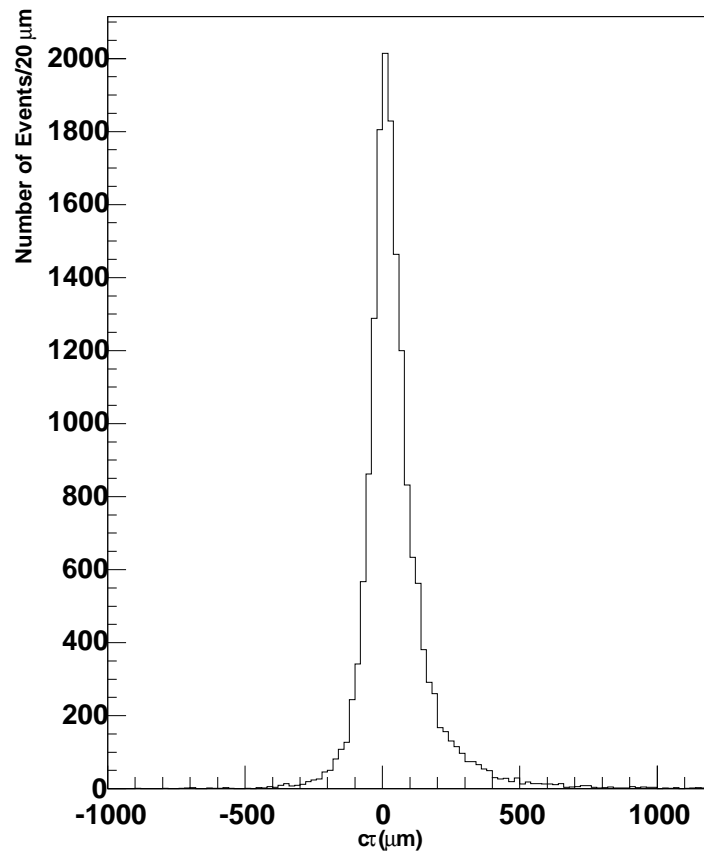


Figure 3.12: Proper decay length of background event

Table 3.3: List of input parameter

$f_{bg}$	$4.43 \pm 0.01$
$\tau_{bg}$	$46 \pm 1$
$\alpha$	$0.964 \pm 0.001$

### 3.7 Lifetime calculation

After the all cut, there are 1349690 candidates of 1-3 topology. Shown in figure 3.13 is decay length distribution of all candidates. We obtain the mean decay length,  $\tau_m$  is ,

$$c\tau_m = 83.17 \pm 0.10 \mu m \quad (3.12)$$

After the background estimation , 95.57% of the events in the sample are tau events. We correct the reconstructed proper decay length using equation 3.8.

As a result, lifetime of the tau lepton is

$$c\tau_\tau = 88.60 \pm 0.19 (\mu m) \quad (3.13)$$

$$\tau_\tau = (295.62 \pm 0.64) \times 10^{-15} (s) \quad (3.14)$$

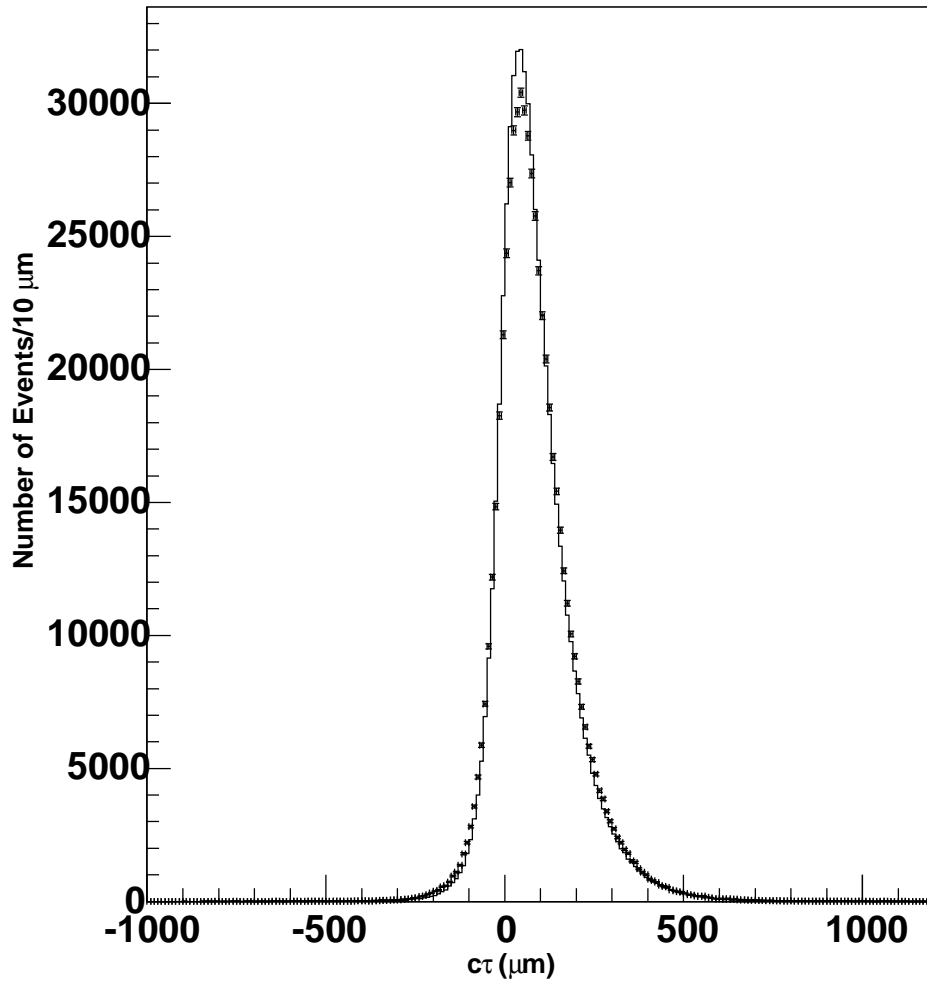


Figure 3.13: Decay length( $c\tau$ ) distribution of data and Monte Carlo. Data are indicated by points with error bars, Monte Carlo( $\tau$ -pair and BG) by the solid histogram.

### 3.8 Systematic Errors

In this section, we estimate the size of systematic effects. We determine systematic errors from interaction point (IP), background fraction, and background lifetime by varying these parameters by  $\pm 1\sigma$  and measuring the average difference in  $c\tau_\tau$  in the

data. The average systematic uncertainty in  $\tau_\tau$  due to a  $1\sigma$  effect is defined as

$$\sigma_{sys} = \frac{1}{2} |c\tau_\tau(+\sigma) - c\tau_\tau(-\sigma)|. \quad (3.15)$$

### 3.8.1 Interaction Point (IP) and Vertex

We determine a  $1\sigma$  systematic error from all beam uncertainties and vertex uncertainties by  $1\sigma$  in  $x$  and  $y$ . We obtain a  $1\sigma$  systematic error by adding in quadrature the individual systematic effects. We obtain  $0.22 \mu m$  as the total systematic error from IP (table 3.4) and  $0.42 \mu m$  from vertexing.

### 3.8.2 Background fraction and lifetime

In the case of background fraction ( $f_{bg}$ ), there is big uncertainties. We determine the systematic error from background fraction by varying  $f_{bg}$  by  $\pm 1\%$ , and measure the error using equation 3.15 .

Systematic errors from background fraction and lifetime are listed in table 3.4

### 3.8.3 Summary

Combining these systematic errors, we obtain the overall systematic error,  $\sigma_{sys}$

$$\sigma_{sys} = 0.63\mu m \quad (3.16)$$

Table 3.4: List of systematic errors.

	$\sigma_{sys}(\mu m)$
$IP_x$	0.18
$IP_y$	0.12
$IP$ total	0.22
$Vertex_x$	0.26
$Vertex_y$	0.33
$Vertex$ total	0.42
BG fraction ( $f_{bg}$ )	0.49
BG lifetime ( $\tau_{bg}$ )	0.02
$total$	0.63

## Chapter 4

# Conclusion

We have measured tau lepton lifetimes using  $98.9 \text{ fb}^{-1}$  of  $e^+e^-$  data collected with the BELLE detector near the  $\Upsilon(4S)$  resonance. We obtain the lifetime,

$$\tau_\tau = (295.62 \pm 0.64 \pm 2.10) \times 10^{15} \text{ sec}$$

where the first error is statistical and the second is systematic. The Standard Model predicted tau lifetime is  $\tau_\tau = (291 \pm 1) \times 10^{-15} \text{ sec}$  while the current world average of tau lifetime is  $\tau_\tau = (290.6 \pm 1.1) \times 10^{-15} \text{ sec}$ . Shown in figure 4.1 is a comparison of this analysis result with recent measurements. Our measurement is  $2 \sigma$  higher than the tau lifetime predicted by the Standard Model.

We can obtain the smaller statistical error because of large tau data set. For more accurate result, we have to check the systematic error more precisely.

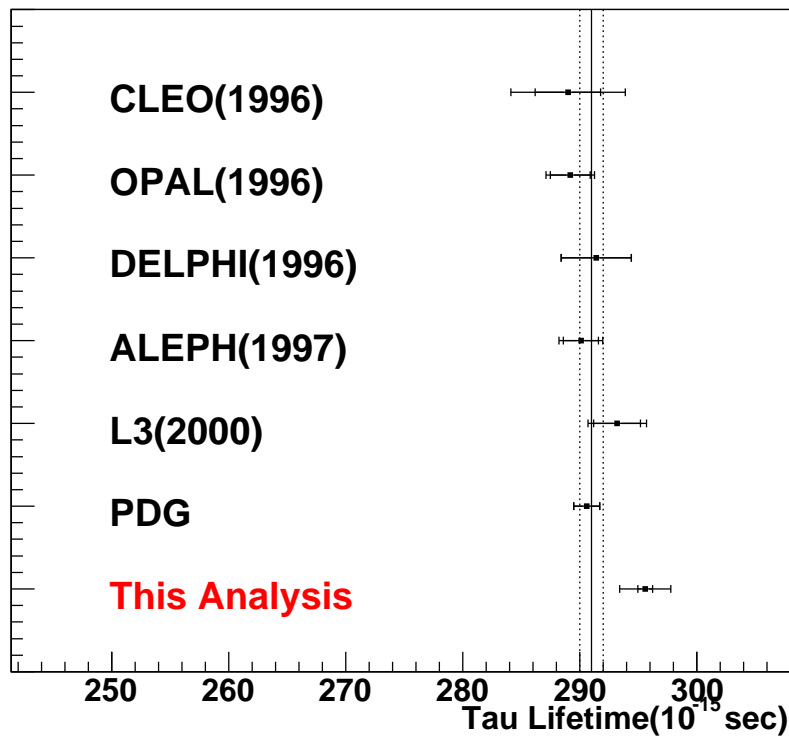


Figure 4.1: List of measured tau lifetime result. Standard Model predicted lifetime is also shown(line).

# Bibliography

- [1] R.Balest *et al.* , CLEO Collaboration, Phys.Lett. B 388, 402(1996).
- [2] J.Whitemore, Ph.D.thesis, Ohio State University (1992) unpublished.
- [3] W.J.Marciano and A.Sirlin Phys. Rev. Lett.61, 1815(1988).
- [4] J.Tanaka, Belle note 194(1998) unpublished.
- [5] G.Alimonti *et al.*, Nucl. Instr and Meth. A453(2000)71; Belle SVD Group, “Technical Design Report of Belle SVD”(1998.)
- [6] H.Hirano *et al.*, Nucl. Instr and Meth. A455(2000)294; M.Akatsu *et al.*, Nucl. Instr and Meth. A454(2000)322.
- [7] T.Iijima *et al.*, Nucl. Instr and Meth. A453(2000)321.
- [8] TH.Kichimi *et al.*, Nucl. Instr and Meth. A453(2000)315.
- [9] H.Ikeda *et al.*, Nucl. Instr and Meth. A441(2000)401.
- [10] A.Abashian *et al.*, Nucl. Instr and Meth. A449(2000)112
- [11] Belle Collaboration, “Belle progress report 1995 April - 1996 March”, KEK Progress Report 96-1(1996).
- [12] R.Brun *et al.*, GEANT 3.21, CERN Report No.DD/EE/84-1(1987).
- [13] J.Jadach and Z.Was, Comp. Phys. Commun 85(1995)453.
- [14] CLEO software document homepage:  
<<http://www.lns.cornell.edu/public/CLEO/soft/qq/index.html>>(1998).
- [15] Belle aafhb document homepage:  
<[http://belle.kek.jp/secured/tautp/aafhb\\_readme.html](http://belle.kek.jp/secured/tautp/aafhb_readme.html)>(1999).
- [16] Review of Particle Physics,D.E.Groom *et al.*, Eur. Phys. J.C 15(2000)1.
- [17] K.Hanagaki *et al.*, Nucl. Instr and Meth. A485(2002)490.

- [18] A.Abashian *et al.*, Nucl. Instr and Meth. A491(2002)69.

# Acknowledgment

Feb 2005  
Satoru Nozaki

I would like to thank everyone who helped me.

First, I would like to thank my advisor, Prof. H. Yamamoto for introducing me to the BELLE experiments and his guidance. I would like to Prof. A. Yamaguchi and Dr. Nagamine for their valuable advice. Staffs in the Research Center for Neutrino Science and in KEK and BELLE collaborators helped me so much.

I would like to thank students in RCNS for their cooperation, and for many discussions with them.

Finally, I would like to thank my family for their continuous support and encouragement.